The Flux Ratio of a Jet to Its Counterjet Revisited

Gang Bao & Paul J. Wiita

Department of Physics & Astronomy,
Georgia State University, Atlanta GA 30303, USA
bao(wiita)@chara.gsu.edu

ABSTRACT

A general relativistic formula for the flux density ratio of a nuclear jet to its counterjet is obtained. The key general relativistic effect, i.e., light bending by the black hole, favors the visibility of the counterjet. The formula is significantly different from the one considering only Doppler effects when the angle between an line of sight and the jet, i, is small, say $i < 10°$. It is found that gravitational lensing plays a vital role if $i \sim 1°$ though the probability of this effect dominating is small. It is possible for a counterjet to be visible even if the jet has a high value of Lorentz factor, γ. Lensed counterjets will only be visible for subluminal sources.

We apply the more general formula to the recently observed counterjet in NGC 1275 and show that the value of i is slightly smaller than when derived by the traditional formula. For reasonable assumptions about other parameters we set limits on the viewing angle of $i > 16°$, and on the spectral index of $\alpha < 1.6$.

Subject headings: accretion, accretion disks — black hole physics — galaxies: active — galaxies: individual (NGC 1275, NGC 5128) — galaxies: jets — gravitational lenses

1. Introduction

It is believed that most jets in radio galaxies, quasars, and blazars are intrinsically symmetric, i.e., in general there exists a pair of oppositely directed jets of comparable strength and velocity, although observations of radio galaxies and quasars generally reveal a strong asymmetry in the surface brightness of the nuclear radio source (e.g., Wilkinson 1995). Most powerful sources show only a one-sided jet on both sub-parsec and multi-kiloparsec scales (e.g., Bridle & Perley 1984; Gopal-Krishna & Wiita 1997); presumably only the jet pointing towards us is observed. The reason for this is that for relativistic flows the approaching jet is strongly enhanced by the Doppler effect, while the receding counterjet is dimmed (e.g., Scheuer & Readhead 1979; Blandford & Königl 1979), and their brightness ratio is so large that the counterjet usually cannot be identified in radio maps of the highest feasible dynamic range. Recently, nuclear counterjets in NGC 1275 (3C 84; Vermeulen, Readhead, & Backer 1994; Walker, Romney & Benson 1994) and in NGC 5128 (Centaurus A; Jones et al. 1996) have been apparently resolved by Very Long Baseline Interferometer (VLBI) and in particular by using the Very Long Baseline Array (VLBA) at relatively high radio frequencies. These detections support the the standard twin-beam model of radio sources in active galactic nuclei (AGN) and could provide strong constraints on the kinematics of the radio jet and the nature of the nuclear atmosphere. Such observations can be of great relevance for understanding both the unification schemes (for recent reviews see Gopal-Krishna 1995; Urry & Padovani 1995) and variability (e.g., Wagner & Witzel 1995; Marscher 1996) of radio loud AGN, which are based on beaming and orientation arguments.

Traditionally a formula including only special relativity (SR) is used to obtain estimates of some important parameters such as the angle between the line of sight and the jet direction and the velocities of the emitting regions, from observations of (or limits to) the flux ratio of the jet to the counterjet, the apparent velocities of components, and the spectral index of the emission. In this paper, we provide a more accurate formula which includes all special and general relativistic (GR) effects. We consider the possibility that the emitting region seen as the nuclear counter jet is behind the supermassive black hole presumed to lie at the center of AGN (e.g., Rees 1984), so the radio emission from the counterjet can be influenced strongly by the black hole if the angle between the line of sight and the jet direction is small; in other words, radio photons from the base of the counterjet have to pass close to the black hole in order to reach us, and thus their trajectories will be highly curved. This may modify the results derived in the traditional way. When the angle between the line of sight and the jet direction is very small this phenomenon makes the apparent image of the counterjet appear both further away from the black hole and brighter; this possibility was mentioned but not calculated by Rauch & Blandford (1994). Then the traditional formula for the brightness ratio, derived ignoring gravitational effects, will not be valid and should be replaced by a fully GR one.

In §2 we present the formulae needed to obtain the jet to counterjet flux ratio and the location of the apparent image of the counterjet, along with a discussion of the formulae and the general results. In §3, we perform some calculations relevant to the counterjet in NGC 1275. Our conclusions and some caveats are given in the last section.

2. The jet/counterjet flux ratio

As is usually done, we assume that both the jet and the exactly oppositely directed counterjet contain a series of apparently separate knots of radio-emitting plasma (e.g., Scheuer & Readhead 1979), which move along the jet/counterjet at an angle i relative to the observer at infinity (see Fig. 1), and that the jet and counterjet are intrinsically identical. For simplicity, we assume that the observed pattern speed and bulk velocities of the shocks in the jet that presumably have produced the plasma knots are the same (see e.g., Ghisellini et al. 1993), and perform an analysis for a Schwarzschild central black hole.

2.1. The formalism

Let us start with the geodesic motion of photons in Schwarzschild geometry. The four velocity of the photon can be written as

$$u^t = \xi^{-1}, \tag{1a}$$

$$u^r = \left[1 - \xi(\frac{B}{r})^2\right]^{1/2}, \tag{1b}$$

$$u^\theta = r^{-2}\left(B^2 - L^2/\sin^2\theta\right)^{1/2}, \tag{1c}$$

$$u^\varphi = r^{-2}L/\sin^2\theta, \tag{1d}$$

where B is the total impact parameter of the photon, L is the impact parameter around the symmetry axis and $\xi = 1 - 2/r$; units where $c = G = M_{BH} = 1$ are used. In Schwarzschild space-time the two parameters B and L are not independent (Bao 1992) and in our case we can, without loss of additional generality, choose $L = 0$, so there is no φ motion. Any four-vector $f^{(\mu)}$ in a static frame may be obtained through a Lorentz transformation from the vector in the comoving frame of the plasma knot (for details, see Bao, Wiita, & Hadrava 1996),

$$f^{(\mu)} = \Lambda^{(\mu)}_{\hat{\nu}} f^{\hat{\nu}}, \tag{2}$$

where " $\hat{\nu}$ " and "(μ)" respectively refer to the quantity measured in the comoving frame of the knot and in the static frame. For knots with bulk velocity v in a radial direction, as measured by a static observer, we simply have

$$\Lambda^{(\mu)}_{\hat{\nu}} = \begin{pmatrix} \gamma & \gamma v & 0 & 0 \\ \gamma v & \gamma & 0 & 0 \\ 0 & 0 & 1 & 0 \\ 0 & 0 & 0 & 1 \end{pmatrix},$$

where $\gamma = (1 - v^2)^{-1/2}$ is the Lorentz factor of the plasma knot.

2.2. The redshift factor and the jet/counterjet flux ratio

The redshift factor, $\mathcal{D}$, is defined as the ratio of the energy measured at infinity to the energy measured at the comoving frame of the knot, i.e.,

$$\mathcal{D} = \frac{p^t(\infty)}{p^{\hat{t}}(r)}, \tag{3}$$

where p^ν and $p^{\hat{\mu}}$ are the four-momentum of the photon. According to the above formulae we have

$$\mathcal{D} = \frac{\xi^{1/2}}{\gamma} \frac{1}{1 \pm v(1 - \xi(\frac{B}{r})^2)^{1/2}} \tag{4}$$

where the $+$ and $-$ in the denominator respectively refer to the case of the knot receding from or moving towards us.

If the solid angle subtended by the source is Ω, and the observed intensity is $I_\nu(\nu)$, which will be assumed to be adequately approximated by a power-law form with spectral index α, i.e., $I_\nu \propto \nu^{-\alpha}$, the observed flux density is,

$$S_\nu = I_\nu \Omega = \mathcal{D}^{3+\alpha} \hat{I}_{\hat{\nu}}(\nu)\Omega. \tag{5}$$

The differential solid angle $d\Omega$ can be expressed in terms of the total impact parameter, B, of the photon

$$d\Omega = \frac{B\ dB\ d\phi'}{d^2},$$

where d is the distance between the observer and the emitting matter, and ϕ' refers to the angular position of the jet and counterjet in the observer's sky; $d\Omega$ can be rewritten in terms of the coordinates of the jets r and φ as

$$d\Omega = \frac{B}{d^2}\left|\frac{\partial(B, \phi')}{\partial(r, \varphi_s)}\right| dr d\varphi,$$

where $\varphi \sim \pi$ for a counterjet and $\varphi \sim 0$ for a jet. The Jacobian only contains $\partial\phi'/\partial\varphi$ and $\partial B/\partial r$ terms; the former is found to be

$$\frac{\partial\phi'}{\partial\varphi} = \frac{\cos i}{1 - \sin i^2 \cos\varphi^2},$$

and the latter can be found from

$$\frac{\partial r}{\partial B} = \frac{\sqrt{2u_s^3 - u_s^2 + B^{-2}}}{u_s^2 B^3} \int_0^{u_s} \frac{du}{\sqrt{(2u^3 - u^2 + B^{-2})^3}},$$

where $u_s = r^{-1}$. When there exists a periastron p on the trajectory of a photon, $\partial r/\partial B$ can be expressed in terms of the first and second elliptical integrals (Bao, Hadrava, & Østgaard 1994).

Henceforth, we refer to the jet as "1" and the counterjet as "2". The ratio of the observed flux density of the jet to the counterjet is then

$$R = R_D \; R_\Omega, \tag{6a}$$

where

$$R_D = \left[\frac{1 + v_2(1 - \xi_2(\frac{B_2}{r_2})^2)^{1/2}}{1 - v_1(1 - \xi_1(\frac{B_1}{r_1})^2)^{1/2}} \frac{\gamma_2}{\gamma_1} \frac{\xi_1}{\xi_2} \right]^\eta \frac{\hat{I}^1_{\hat{\nu}}}{\hat{I}^2_{\hat{\nu}}}, \tag{6b}$$

and

$$R_\Omega = \frac{\Omega_1}{\Omega_2}, \tag{6c}$$

with $\eta = 3 + \alpha$ for individual knots ($\eta = 2 + \alpha$ for continuous flow; e.g., Scheuer & Readhead 1979).

2.3. The apparent image of the counterjet

It is traditionally assumed that the jet and the counterjet are intrinsically identical, with any observed differences arising from Doppler boosting and light-travel time effects (e.g., Vermeulen & Cohen 1994; Gopal-Krishna & Wiita 1997). But we write R in the form of the factors in equation (6), to stress that even when the counterjet and jet have comparable luminosities and seem to have comparable scales, the counterjet is generally closer to the black hole than it appears because of light bending by the black hole, as illustrated in Fig. 1. It is obvious that the location of the main image of the counterjet is a function of the viewing angle (or inclination), i, as well as its actual location, r_2.

The apparent location of the image of counterjet depends on the photon impact parameter $B_2(r_2, i)$, and for a static counterjet,

$$r_{amp} = \frac{B_2}{r_2} \frac{1}{\sin i}, \tag{7a}$$

$$r_{2,app} = r_{amp} r_2 \sin i = B_2, \tag{7b}$$

where r_{amp} is the location of the image of the counterjet expressed in units of r_2, the actual distance, and the apparent position of the emitting region, $r_{2,app}$, takes into account the projection onto the plane of the sky. Fig. 2 shows how the amplified location of the principal image of the counterjet depends on the inclination i and its source location r_2. For a given inclination, if r_2 is smaller, then r_{amp} is bigger, while for a given r_2, a smaller i corresponds to a bigger r_{amp}. For large i and r_2, r_{amp} and $r_{2,app}$ approach r_2, i.e., the apparent image coincides with the source. As we clearly see, when the observer is very closely aligned with the jet, e.g., $i \sim 1^\circ$ or less, the apparent location of the main image of the counterjet can be as large as $r_{amp} \sim 10^3 r_2$, though $r_{2,app}$ is still strongly foreshortened by the basic projection effect. So if we see a counterjet at a projected distance of $\sim$ 1pc, and it happens to be seen at viewing angles of $\sim 1^\circ$ or less, then the real distance of the counterjet from the black hole could be much smaller than it appears. For example, if the amplified image of a counterjet is at $10^4 r_s$ and the projected one at some 100's of r_s (where $r_s = 2GM/c^2$) then the real source may be located at only $\sim 10 r_s$ (assuming the central mass, $M_{\rm BH} \gtrsim 10^8 M_\odot$ so $r_s \gtrsim 10^{-5}$pc, thereby setting a large enough physical scale).

It can be seen from equation (6) that two factors which favor the visibility of the counterjet play important roles in the flux density ratio R. First, we consider the ratio of $\gamma_2(r_2)/\gamma_1(r_1)$. We will allow for the possibility that r_2 can be small, e.g., $r_2 \sim (10-100)r_s$. At such a location close to the black hole the jet has probably just begun to be accelerated and collimated (e.g., DeFelice & Carlotto 1996; Sikora et al., 1996), so the value of $\gamma_2(r_2)$ may not exceed unity by very much, while $\gamma_1(r_1)$ may have already reached a high asymptotic value, i.e., $\gamma_1(r_1) \sim 10$, so the ratio of γ_2 to γ_1 could be the order of 0.1. If we assume the plasma knots have a spectral index of $\alpha = 0.5$, the contribution from the γ ratio to R will be $10^{-3.5}$, but this in itself cannot compete with the Doppler and gravitational shifts in R_D when the inclination is small enough. Second, we examine the ratio of the solid angle, R_Ω. If a photon goes along a straight line, then R_Ω will be a constant no matter what the inclination is; and if the emitting regions of the jets are identical, then it will be unity. But this is not true if photons go along a curved path. Photons from the jet reach us on essentially straight paths, but photons from the counterjet, which is behind the black hole relative to the distant observer, will reach us along strongly curved trajectories. The bent trajectories make the source appear bigger and thus brighter.

Traditionally, R_Ω is ignored in estimating the ratio of the jet and counterjet, but this lead to substantial errors if the jet points very close to us. When we ignore the effect of gravity on photon paths, our formulae (4), (6), and (7) can be easily reduced to the traditionally used ones. In this case, the impact parameter can be written as $B = r\sin i$, and $\xi = 1$, so we then have

$$r_{amp} = 1, \qquad r_{2,app} = r_2 \sin i, \tag{8}$$

$$\mathcal{D} = \frac{1}{\gamma(1 \pm v\cos i)}, \tag{9}$$

and for intrinsically identical jets we have

$$R_{SR} = \left[\frac{1 + v\cos i}{1 - v\cos i}\right]^{\eta}. \tag{10}$$

In the above discussions, for simplicity, we have assumed that $\hat{I}^1_{\hat{\nu}}/\hat{I}^2_{\hat{\nu}} = 1$. This is unlikely to be the case in a real situation, particularly if $r_1 \gg r_2$, but the difference typically will not be as influential in the overall ration R as are the others discussed above.

Fig. 3 describes how equation (6) differs from equation (10) as a function of the angle between line of sight and the jet. Fig. 3a refers to the case where the Lorentz factors, α and r_1 are taken as fixed, while r_2 varies by a factor of 100. Naturally, the difference between R and R_{SR} depends on location of the counterjet, and the closer the source of the counterjet is to the black hole, the bigger the difference between R_{SR} and R, because the GR effect is stronger on photons emitted by a source closer to the black hole. Fig. 3b shows the case where the locations of both emission regions, η, and γ_1 are fixed, but γ_2 is allowed to vary from 3 to 8. Smaller counterjet Lorentz factors make for bigger differences between R and R_{SR}, as can be seen from the formula for R_D. Fig. 3c presents the case where both locations and velocities are fixed but η varies from 2.0 (an effective minimum) to 3.5. Although R_{SR}/R depends on η, the dependence is not as strong (for this reasonable range) as it is for plausible ranges in r_2 and γ_2. We note that in all cases, $R_{SR}/R > 1$, and that the difference between SR and GR results becomes smaller when the angle i increases. This is simply because for larger i the bending of light by the black hole is weaker, and SR boosting and dimming are dominant.

Fig. 4 and Fig. 5 present the ratios of R_D, R_Ω, and R as a functions of i. In Fig. 4, $\gamma_1 = 10$, $\gamma_2 = 1.1$, $r_2 = 10r_s$, and $r_1 = 10^3 r_s$, while η varies from 2.5 to 3.5. In Fig. 5, the same γ's are assumed, with $\eta = 3.0$, and $r_1 = 10^4 r_s$ also fixed, while r_2 ranges from $(5 - 500)r_s$. The ratios R_D, R_Ω, and their observed product R, depend strongly on r_2 and η. Small values of η favor the visibility of the counterjet. This is because the combined Doppler and gravitational redshift ratio, R_D, is reduced, while the solid angle ratio remains the same because the bending is independent of η. Although smaller values of r_2 increase R_D, they reduce R_Ω even more, implying that light bending becomes more and more important, and the the final ratio R decreases. We notice that the γ ratio in R_D cannot compete with the Doppler and gravitational effects. In all cases, when i is extremely small, R_Ω declines very rapidly and becomes dominant, so R can become ~ 10 or even smaller. Note that for large inclinations R_Ω approaches unity, implying that bending is not important, and that photon trajectories from the counterjet can also be treated as straight lines.

3. The counterjets in NGC 1275 and NGC 5128

A radio component on (projected) parsec scales to the north of compact core as well as the long known one to the south was revealed by the high dynamic range VLBA image at 8.4 GHz of the radio source in NGC 1275 (Walker et al. 1994) and it was independently detected at 22 GHz (Vermeulen et al. 1994). More recently, a sub-parsec scale counterjet has also been detected in the nucleus of the closest radio galaxy, Centaurus A (NGC 5128), with VLBI imaging at 2.3 and 8.4 GHz (Jones et al. 1996). Both can be explained by two oppositely directed, symmetric relativistic jets. Individual components have been measured with the observed velocity, v_{app}, up to $\sim 0.25\ h^{-1}c$ ($H_0 = 100h$ km s^{-1} Mpc^{-1}) for NGC 1275 and around $0.66c$ for NGC 5128, suggesting that the physical velocities need not be extremely close to the speed of light. In addition, the newly discovered components (the counterjets) have inverted spectra; this is most likely due to free-free absorption by some gas (perhaps an accretion disk) around the black hole.

Given the implicitly assumed presence of relativistic velocities, our calculations indicate that subluminal motion with observable double-sided jets can only happen in two cases. The first is the "normal" situation where SR effects dominate and the inclination of the jet is relatively large ($i \gtrsim 30°$). The second, when GR effects dominate, requires the jet to be be extremely close to the line of sight, and also that the nuclear environment, such as the accretion disk, does not absorb too much of the radiation from the counterjet. In both cases, the observed transverse velocity, v_{app}, can be under the speed of light, and the observed jet/counterjet brightness ratio R can fall to the order of 10, roughly the value seen for NGC 1275 and NGC 5218. We recall that one-sidedness is usually accompanied by apparent superluminal motion (e.g., Vermeulen & Cohen 1994), implying that for such sources the jets are generally moderately away from the jet direction, e.g., $\sim 1/\gamma$ radians, where the brightness ratio is usually more than 10^2, and counterjet detection is very difficult or impossible if $\gamma \sim 10$.

In the case of extremely small i, one could see the counterjet only through photons which reach us by strongly curved trajectories and what is observed is the apparent image of an emitting region which is actually substantially closer to the black hole, even after projection effects are taken into account. A very small i allows the motion in the jet to be observed as subluminal even with the γ of the jet being of the order of 10, as seems to be common in many AGN (e.g., Vermeulen & Cohen 1994) and is expected from many theoretical arguments (e.g., Abramowicz, Ellis, & Lanza 1990; Sikora et al. 1996). Moreover, for a small inclination, the radiation from the counterjet will have a higher probability of penetrating the accretion disk, yielding partial absorption and a change in the observed spectral index between the jet and counter-jet, than it would for a large inclination. Of course the a priori probability of a source having such a small i is very low, but this is not inconsistent with the observation of so few counterjets despite many deep searches.

Still, the likelihood that any counterjets observed to date involve near-field lensing is small, and would imply other coincidences are involved. While the spectra of the jet and counterjet in NGC 1275 are very different, with $\alpha_8^{22} \approx 0.6$ for the jet and $\alpha_8^{22} \approx -1.7$ for the counterjet, Vermeulen et al. (1994) argue this is probably not due to synchrotron self absorption, but is more readily explained by free-free absorption affecting the emission of the counterjet. The fact that the counterjet is not detected at all at 1.7 GHz (Biretta et al. 1991) is consistent with free-free absorption. Also, if the emission region identified as the counterjet was really *much* closer to the central source, it would therefore actually be much smaller physically than the emission region identified as the jet, and one might expect the counterjet to be strongly self-absorbed even at these frequencies, though this conclusion is certainly quite dependent on the details of the model. It would also be unlikely that the intrinsic intensities were at all similar in such a scenario (while this is not a necessary part of the general GR scenario, the calculations we have done do assume this is the case, for simplicity). Finally, strong lensing should produce a significantly distorted image, i.e., a circular source may appear as banana shape perpendicular to the line of sight. While the morphologies of the jet and counterjet are certainly different in NGC 1275 (Vermeulen et al. 1994; Walker et al. 1994), the differences are not immense and certainly are not clearly indicative of gravitational amplification and distortion of the counterjet.

A relatively large angle for i may naturally also satisfy the two observational limits: i.e, the observed subluminal motion, and the observably low value of R (around 50 at 8.4 GHz) and around 9 at 22 GHz, where absorption is less important, and therefore more likely to reflect the "actual" flux ratio (when boosting and dimming are included but any absorption is absent). But if i is too big then photons from the counterjet may not pass through much more of the free-free absorbing material around the black hole (particularly if it is very compact, like an accretion disk) and this could be inconsistent with the inverted spectra observed (e.g., Levinson, Laor, & Vermeulen 1995).

Although the observed ratio for jet and counterjet in NGC 1275 is not very well defined, Walker et al. (1994) obtained parameters $v \approx 0.33$, $i \approx 30^\circ$ and $\eta \approx 3.7$ (for $h = 1$), by using following three conditions: the ratio of the apparent distances from the core of equivalent components in the approaching and receding jets are determined by time-delay effects, so $D = (1 + v\cos i)/(1 - v\cos i)$; the observed speed of the jet $v_{app} = (v \sin i)/(1 - v\cos i)$; and the formula (10) for R.

When general relativistic effects (and concomitant different velocities) are included (but any possible intrinsic misalignment is still ignored) the above equations must be replaced by the following: the ratio of the apparent distances from the core of equivalent components in the approaching and receding jets

$$D = \frac{B_1(r_1, i)}{B_2(r_2, i)} \frac{1 + v_2 \cos i}{1 - v_1 \cos i}; \tag{11}$$

the apparent speed of the jet (as photons from it basically travel along a straight line)

$$v_{app} = \frac{v_1 \sin i}{1 - v_1 \cos i}; \tag{12}$$

and the more general formula (6) for R. Note that not all parameters of the jet and counterjet satisfy our D-equation (11). If we reasonably require the counterjet to be moving away from us so $v_2 \cos i \geq 0$, then we have a constraint $DB_2 - B_1 \geq DB_2 v_1 \cos i$.

As an example, stay close to the assumption of Walker et al. and let $r_1 = r_2$; choose a large value in geometrical units for both, $10^4 GM/c^2$. In this case r_{amp} is not significantly different from r_2 when i is around 30°. Fig. 6 shows the solution for i by using equations (11) and (12). We use the same observed values of D and v_{app} as did Walker et al. (1994), i.e., $D = 1.8$, $v_{app} = 0.25$ (if $h = 1$; c will be henceforth suppressed), or 0.50 (appropriate if $h = 0.5$ or if higher speeds are detected later). Solutions to equation (11), or D-curves, are shown for $v_2 = 0.34$, 0.20, and 0.10. From Fig. 6, when $v_{app} = 0.25$ and $v_2 = 0.34$ we see that $i = 31.2°$ and $v_1 = 0.34$; while if $v_{app} = 0.50$, $i = 46.8°$, and $v_1 = 0.47$. Our solutions have i slightly less than Walker et al. (1994) derived, $i = 32°$, and $i = 52°$, respectively. We now examine the constraints set by the spectral index (or η). For the case of $v_{app} = 0.25$ and $\eta = 3.7$, we have $R = 9.10$ for $i = 31.2°$. Walker et al. used $R = 9$, and found a good fit for $\eta = 3.7$. According to formula (6), if $v_2 \leq v_1$, in order to have the jet/counterjet-flux ratio $R \sim 9$, we must increase η for a smaller i if $r_1 = r_2$.

If there were no bending of light rays from the counterjet of NGC 1275, and the jets were intrinsically similar, then it could be that $r_1 = r_2$ and $v_1 = v_2$. But if bending exists, then it is most probable that $r_1 > r_2$ and $v_1 > v_2$. As we see from Fig. 6 and Fig. 7, where $r_2 = 0.8 r_1$ but other parameters are unchanged, by decreasing r_2 we obtain larger values of i but by decreasing v_2 we have smaller values of i. So, an extreme case for the source would correspond to the solution where $r_1 = r_2$, $v_2 = 0$ and for $v_{app} = 0.25$. First solve for $r_1 = 10^4 GM/c^2$; the solution is $i = 17°$, and $v_1 = 0.47$. Then consider $r_1 = 10^3 GM/c^2$, which is a reasonable lower limit for the jet scale in this source; then $i = 16.2°$, and $v_1 = 0.48$. As the smallest angle is a weak function of r_1 (unless the lensing is extreme), we set a limit for NGC 1275,

$$i > 16°.$$

Also, for this case we find $\eta = 4.6$ if we require the flux ratio of the jet to its counterjet to be 9. So, we also have a rough (and not terribly interesting) limit for the spectral index

$\alpha < 1.6$. The opposite limits on i and α cannot be obtained because of the very uncertain lower limit to r_2 and upper limit to v_2. Our D-curves are significantly different from the one used by Walker et al. when i is small; this is obviously because of the substantial gravitational effect under these circumstances. Note that the curves for the relatively large r_2 values displayed in Figs. 6 and 7 have second, unphysical, solutions at $i \equiv 0$ and $v_1 \equiv c$! These are not the correct solutions for small i where GR effects dominate but where $r_2 \ll r_1$ that we discussed above.

In that the counterjet in NGC 5128 is only seen at 8.4 GHz and was not detected at all at 2.3 GHz (Jones et al. 1996), and has not yet been observed adequately at higher frequencies, it is more difficult to perform any analysis for this source. The standard analysis yields a large value for the inclination angle $60^\circ \lesssim i \lesssim 77^\circ$, which is supported by the large-scale radio morphology of the source (Jones et al. 1996). For such a large angle any GR effect will be negligible, so equation (10) and the SR relation for D will be adequate to estimate the parameters for the source.

4. Conclusions

We give a more accurate formula to calculate the flux ratio of a nuclear jet to that of its counterjet. All special and general relativistic effects are included, although directly opposed motions are assumed to hold on these sub-parsec scales, and this may not be generally true (e.g., Hough, Zensus, & Porcas 1996). It is found that the ratio, R_{SR}, which considers only Doppler effects, is always larger than the ratio, R, we derived. This means that the key general relativistic effect, i.e., light bending by the black hole, favors the visibility of the counterjet in general. The formula will be significantly different from that of R_{SR} when the angle between line of sight and jet is small, say, when $i < 10^\circ$.

By using formulae (6), (11), and (12) we calculate the case for the observed counterjet in NGC 1275. Our calculation shows when $v_1 = v_2$, the angle between the line of sight and the jet, i, is 31.2° for $h = 1$ and 46.8° for $h = 0.5$ (for $r_1 = 10^4 GM/c^2$). The value of the spectral index is $\alpha = 0.7$ for $h = 1$. The angles are only slightly different from those derived by Walker et al. (1994) because gravitational effects probably do not play a important role in this source. We have considered other solutions when $r_1 \neq r_2$ and $v_1 \neq v_2$. We derived an interesting limit for the angle between the line of sight and the jet for the "standard case", $i > 16^\circ$, and a not particularly interesting upper limit for the spectral index, $\alpha < 1.6$.

General relativistic effects can be dominant when the jet direction almost coincides with our line of sight. In this case, a counterjet is visible because gravitational lensing amplifies its brightness even if the the value of γ of the jet is higher than that of the counterjet. Although the two currently observed nuclear counterjets seem not to require this picture, the possibility of observing a counterjet with an extremely small i should not be summarily dismissed. Since light bending is one of the fundamental properties of black holes, the confirmation of the this effect in a future observation may constitute rather direct evidence that a black hole exists in the source. In order for such small angles to be viable, the projected size of the emitting region would be much less than their physical separations from the core. This condition implies that either extraordinarily massive black holes are involved ($\sim 10^{11} M_\odot$) if actual parsec scales are seen, or higher frequencies and even longer baselines (space VLBI) will be needed to resolve such features on a *much* sub-pc scale for more typically expected black hole masses ($\sim 10^8 M_\odot$).

Strong bending effects happen only when the inclination of the observer is very small, and for such extremely small inclinations, nearly all of the sources will appear subluminal. For large inclinations, where sources also appear subluminal, the brightness ratio R is reduced because the standard special relativistic Doppler effect is weaker. This suggests that counterjets may only be visible in subluminal sources (see Figs. 4 and 5).

Despite the probability of its possessing a smaller Lorentz factor, the possible closeness to the black hole of the region producing the counterjet can enhance its variability in two ways. First, it would probably be more susceptible to intrinsic fluctuations because its smaller physical size. Second, a small motion outwards can dramatically decrease the gravitational amplification (Fig. 4); thus our scenario would typically imply more variability for the counterjet than for the jet. Maps of such sources should be made at multiple epochs to check for this possibility. In addition, since gravitational effects affect the polarization properties, we expect that the observed polarization of the jet and counterjet to differ in a particular fashion if the influence of the nuclear atmosphere is small. In particular, the fractional polarization should be smaller for the counterjet because the bending produces an effective depolarization (Bao et al. 1996). These expected polarization differences also could conceivably provide a way to distinguish between a lensed counterjet and the standard picture. Although these effects are beyond the scope of this current study, they will be considered in the near future, as will the complications introduced by intrinsically misaligned nuclear jets. Finally, we note that a near-field gravitational lens makes the apparent image of the counterjet wider than the real source in the direction perpendicular to the line of sight. Observations of such a morphology may allow us to identify a lensed jet in the future.

We thank Professor F. DeFelice for discussions on some of these formulae, and Professor P. Hadrava, Ms. Y. Xiong, and two anonymous referees, for their valuable comments. Part of this work was done when PJW was at the Aspen Center for Physics. We are grateful for the support this work received from NASA grant NAG 5-3098 and from a Research Program Enhancement grant at Georgia State University.

REFERENCES

Abramowicz, M. A., Ellis, G. F. R., & Lanza, A. 1990, ApJ, 361, 470

Bao, G. 1992, A&A, 257, 594

Bao, G., Hadrava, P., & Østgaard, E. 1994, ApJ, 435, 55

Bao, G., Wiita, P. J., & Hadrava, P. 1996, Phys. Rev. Lett., 77, 12

Biretta, J. A., Bartel, N., & Deng, J. 1991, in IAU Colloq. 131, Radio Interferometry: Theory, Techniques and Applications, ed. T. J. Cornwell & R. A. Perley (ASP Conf. Ser. 19; San Francisco: ASP), 334

Blandford, R. D., & Königl, A. 1979, ApJ, 232, 34

Bridle, A. H., & Perley, R. A. 1984, ARA&A, 22, 319

DeFelice, F. & Carlotto, L. 1996, MNRAS, submitted

Ghisellini, G., Padovani, P., Celotti, A., & Maraschi, L. 1993, ApJ, 407, 65

Gopal-Krishna 1995, Proc. Nat. Acad. Sci. (USA), 92, 11399

Gopal-Krishna, & Wiita, P. J. 1997, in Active Galactic Nuclei, Dense Stellar Systems, and their Environment, ed. S. Lamb, & J. Perry (ASP Conf. Ser.; San Francisco: ASP), in press

Hough, D. H., Zensus, J. A., & Porcas, R. W. 1996, ApJ, 464, 715

Jones, D. L., et al. 1996, ApJ, 466, L63

Levinson, A., Laor, A., & Vermeulen, R. C. 1995, ApJ, 448, 589

Marscher, A. P. 1996, in Blazar Continuum Variability, ed., H. R. Miller, J. Webb, & J. C. Noble (ASP Conf. Ser.; San Francisco: ASP), in press

Rauch, K. P., & Blandford, R. G. 1994, ApJ, 421, 46

Rees, M. J. 1984, ARA&A, 22, 471

Scheuer, P. A. G., & Readhead, A. C. S. 1979, Nature, 277, 182

Urry, C. M., & Padovani, P. 1995, PASP, 107, 803

Vermeulen, R. C., & Cohen, M. H. 1994, ApJ, 430, 467

Vermeulen, R. C., Readhead, A. C. S., & Backer, D. C. 1994, ApJ, 430, L41

Wagner, S. J., & Witzel, A. 1995, ARA&A, 33, 163

Walker, R. C., Romney, J. D., & Benson, J. M. 1994, ApJ, 430, L45

Wilkinson, P. N. 1995, Proc. Nat. Acad. Sci. (USA), 92, 11342

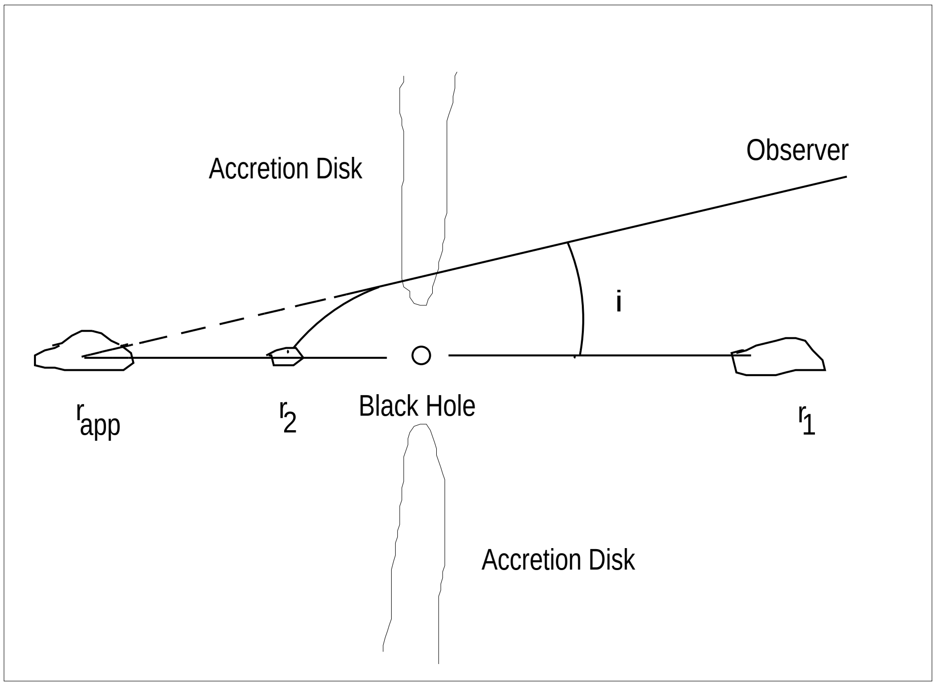

Fig. 1.— Geometry of the jet and the counterjet. The observer has a line of sight that makes an angle i to the jet; r_1 refers to the actual location of the jet, r_2 to that of the counterjet, and r_{amp} to the main apparent image of the counterjet.

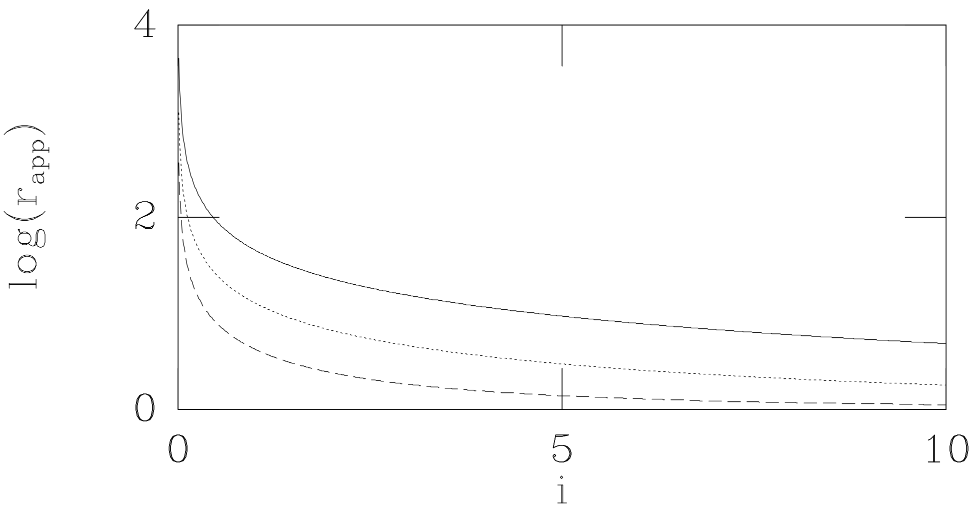

Fig. 2.— The location of the apparent image of the counterjet, r_{amp}, in units of r_2 as a function of inclination i (in degrees). The solid curve refers to $r_2 = 5r_s$ (where $r_s = 2MG/c^2$, with M is the black hole mass), the dotted curve to $r_2 = 50r_s$, and the dashed curve to $r_2 = 500r_s$.

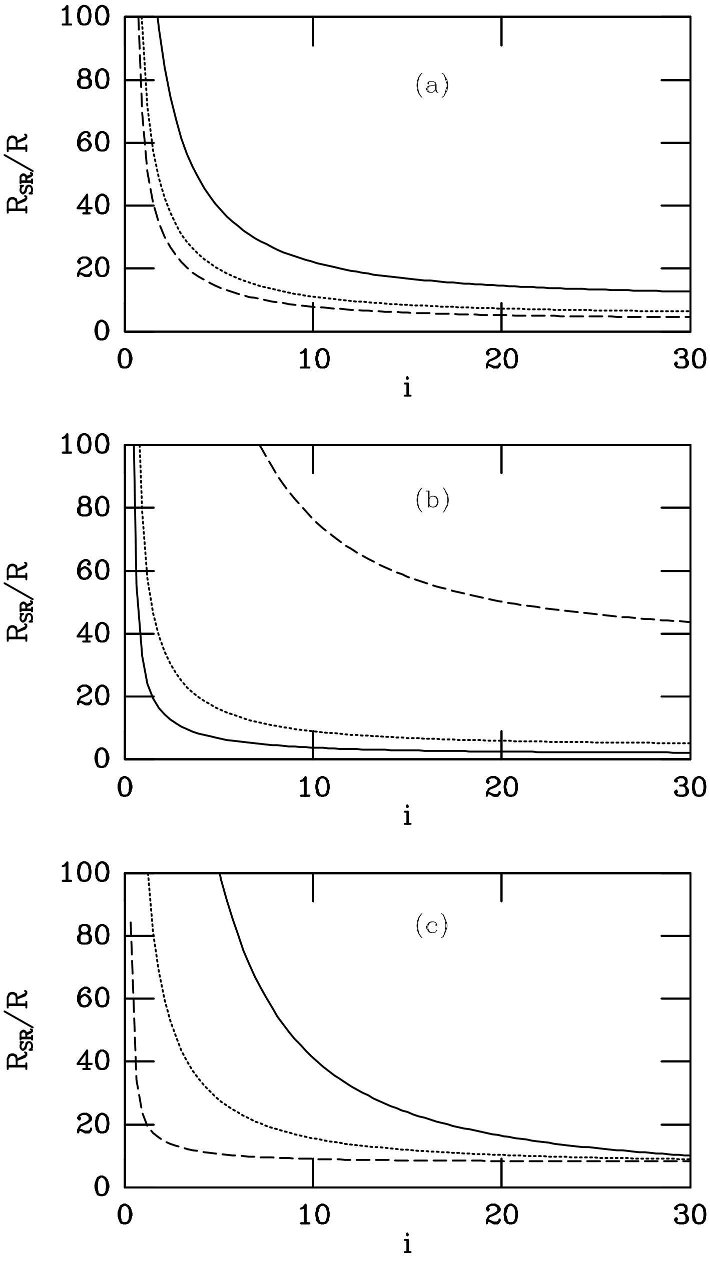

Fig. 3.— The ratio of R_{SR} to R as a function of the angle i (in degrees), between the line of sight and the jet. (a) The case where $\gamma_1 = 10,\ \gamma_2 = 5,\ \ \eta = 3$, and $r_1 = 10^4 r_g$ ($r_g = GM/c^2$); solid curve for $r_2 = 10 r_g$, dashed curve for $100 r_g$, and long dashed curve for $1000 r_g$. (b) The case where $\gamma_1 = 10,\ \ \eta = 3$, and $r_1 = 10^4 r_g$ and $r_2 = 100 r_g$; solid curve for $\gamma_2 = 8$, dashed curve for 6, and long dashed curve for 3. (c) The case where $\gamma_1 = 10,\ \ \gamma_2 = 5$, and $r_1 = 10^4 r_g,\ r_2 = 100 r_g$; solid curve for $\eta = 3.5$, dashed curve for $\eta = 2.5$, and long dashed curve for $\eta = 2$.

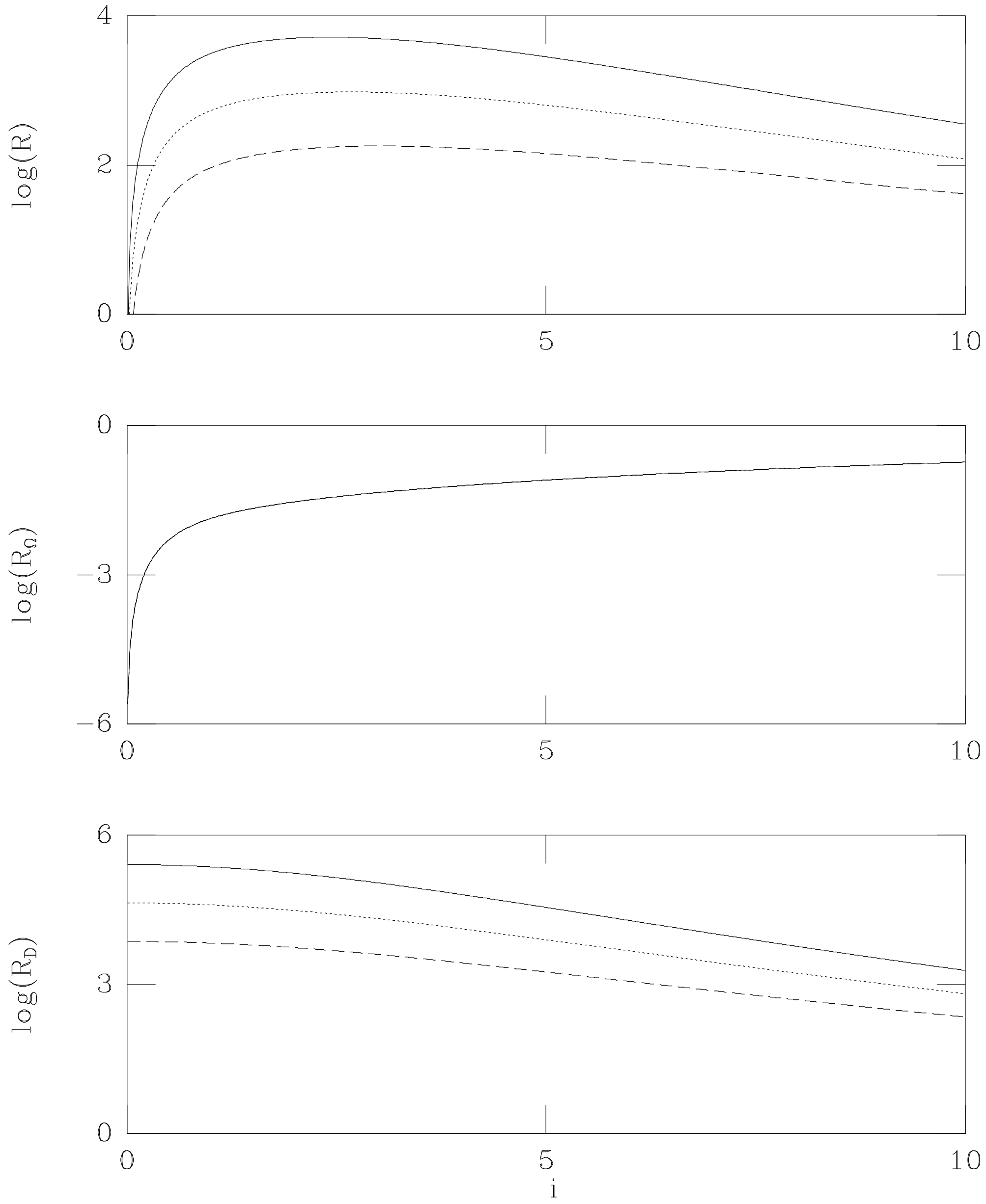

Fig. 4.— The ratios $R_D,\ R_\Omega,$ and R as functions of inclination i, for $\gamma_1 = 10,\ \gamma_2 = 1.1,\ r_2 = 10r_s,\ r_1 = 10^3 r_s$. The solid curve refers to $\eta = 3.5$, the dotted curve to $\eta = 3.0$, and the dashed curve to $\eta = 2.5$.

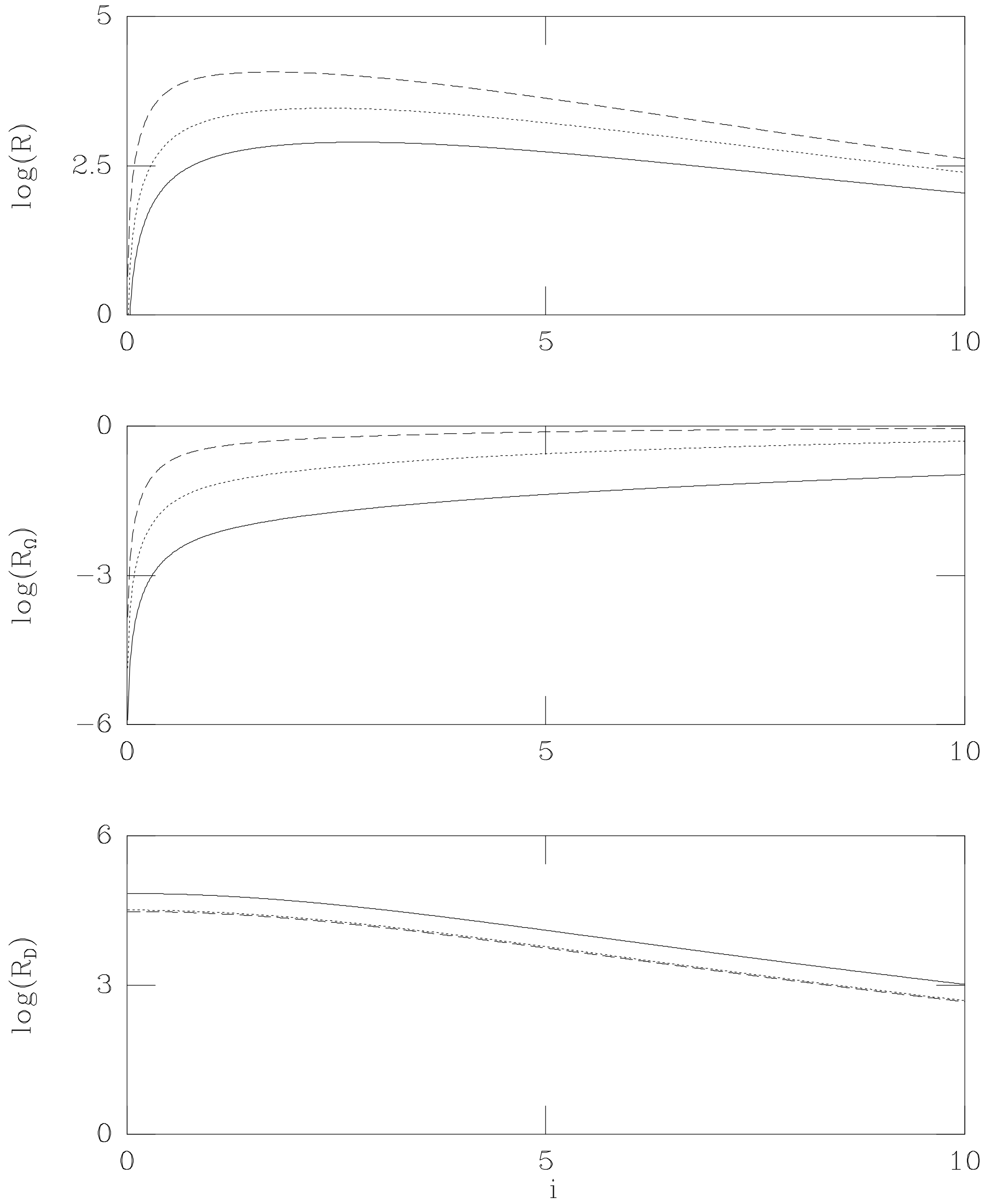

Fig. 5.— The ratios R_D, R_Ω, and R as functions of inclination i, for $\gamma_1 = 10$, $\gamma_2 = 1.1$, $\eta = 3.0$, $r_1 = 10^4 r_s$. The solid curve refers to $r_2 = 5r_s$, the dotted curve to $r_2 = 50r_s$ and the dashed curve to $r_2 = 500r_s$.

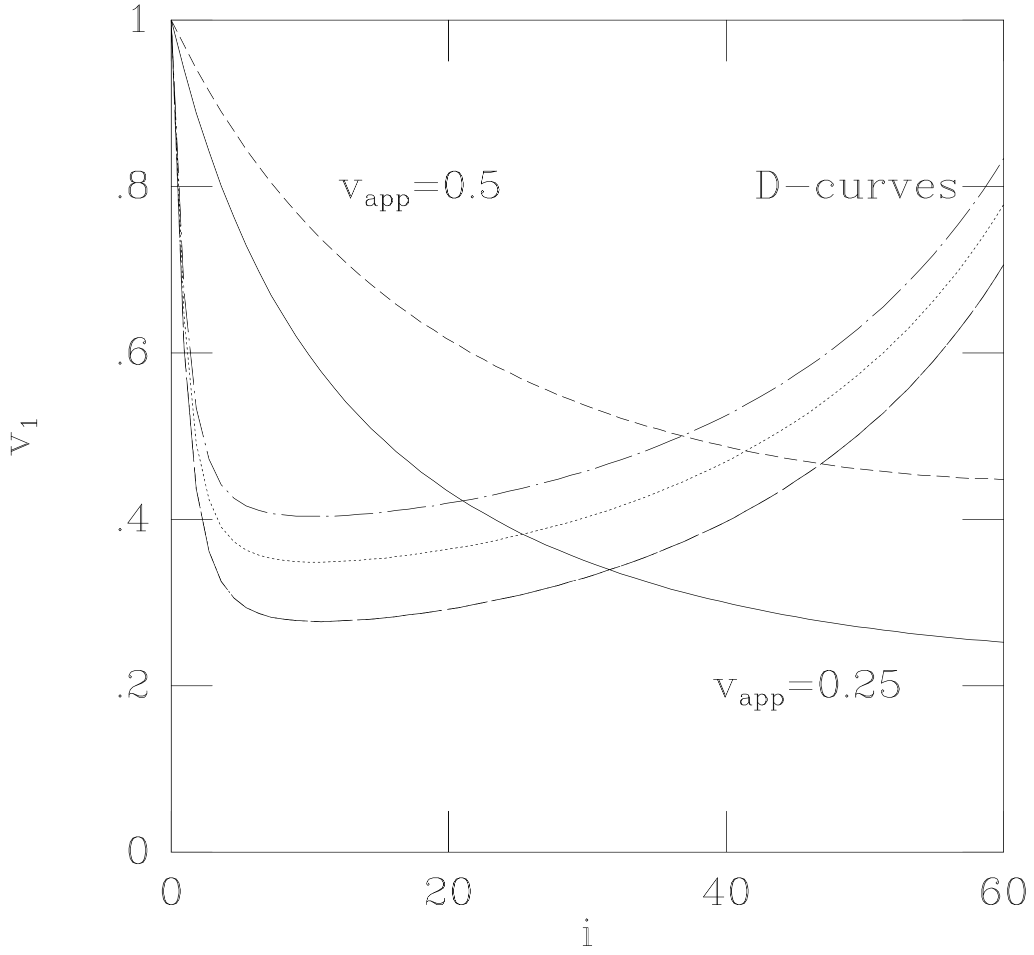

Fig. 6.— Simultaneous solutions of equations (11) and (12) for $r_1 = r_2 = 10^4 GM/c^2$. The solid curve refers to $v_{app} = 0.25$, the dashed curve to $v_{app} = 0.50$, while the long dashed curve, dotted curve, and dash-dotted curve are D-curves with v_2 being 0.34, 0.20, and 0.10, respectively. The crossing points are the solutions for i and v_1.

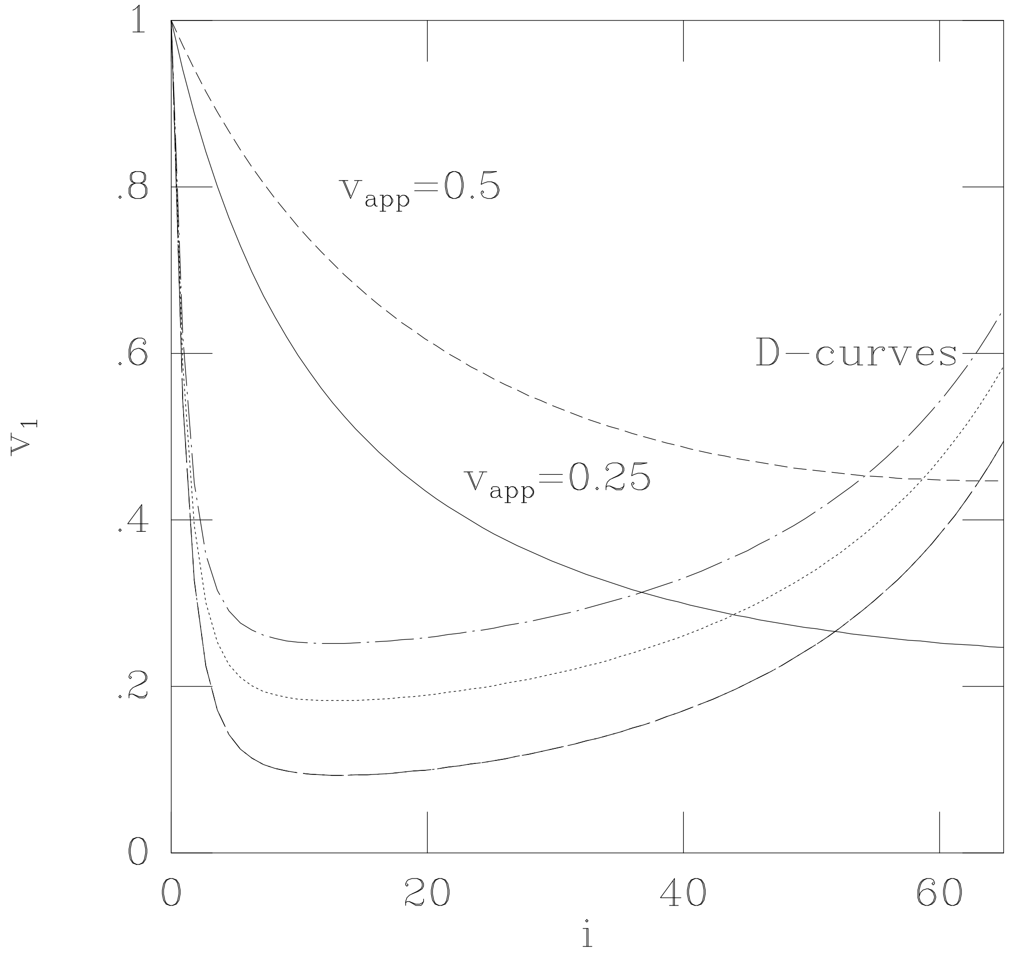

Fig. 7.— Simultaneous solutions of equations (11) and (12) for $r_1 = 10^4 GM/c^2$ and $r_2 = 8 \times 10^3 GM/c^2$. All other parameters and curves are as in Fig. 6.